Experimental Determination of the Deformation Electron Density in Hydrogen Peroxide by Combination of X-ray and Neutron Diffraction Measurements

J.-M. Savariault* [1] **and M. S. Lehmann**

Contribution from the Institut Laue-Langevin, 38042 Grenoble, Cédex, France.
Received June 4, 1979

Abstract: X-ray and neutron diffraction measurements at 110 K have been used to determine the deformation electron density for hydrogen peroxide (H_2O_2). The oxygen atom has been observed to be in a sp^3 hybridization state with one of the lone pairs involved in hydrogen bonding. No charge accumulation has been found in the oxygen–oxygen bond. This is explained as a result of the difference technique used, but does indicate that the transfer of electrons to the binding region is relatively small during bond formation.

Introduction

Since Thenard[2a] in 1818 synthesized hydrogen peroxide (H_2O_2), a great number of experimental and theoretical studies of this compound have been done.[2b] In 1934 theoretical valence calculations by Penney and Sutherland[3] led to the structure of H_2O_2, which was confirmed later by X-ray diffraction[4] and neutron diffraction.[5] The observations showed H_2O_2 to be the smallest molecule which has a barrier of rotation, making it an object of further theoretical studies. One recent quantum-chemical calculation[6] shows that there is no buildup of electron density between the two oxygen atoms.[7] This surprising result as well as the possibility of studying the hydrogen bonding for this very simple molecule led us to undertake the observation of the charge density using diffraction methods. The space group of the crystal is noncentrosymmetric, $P4_12_12$, so in addition we have employed this compound to study the use of noncentrosymmetric crystals for charge-density studies.

Experimental Section

The starting material, a solution of 40% H_2O_2 in water, was purified by distillation under vacuum until a 99% H_2O_2 sample was reached. The pure H_2O_2 was then obtained by fractional crystallization (melting point is −0.43 °C[8]). Drops of pure H_2O_2 were sealed in 0.25- and 0.40-mm diameter Lindemann capillaries for the X-ray study and in 2.5-mm diameter quartz tubes for the neutron study.

X-ray Data Collection. The measurements were carried out at 110 K on a quarter-circle Siemens diffractometer which was controlled by a PDP8 computer. The melting point of H_2O_2 being 0.43 °C, crystals were grown in situ using a cold nitrogen gas flow system. Laue photographs allowed the quality of the crystals to be tested. Two crystals were used: a small one for low-angle measurements and a larger one for high-angle data collection. The orientation and the cell constants at 110 K were determined by least-squares refinement of 28 reflections within the range $20° < \theta < 64°$. Zr-filtered Mo radiation was used and the size of the scan was chosen so that it covered the Mo $K\alpha_1$ and Mo $K\alpha_2$ contributions. The cooling gas flow apparatus does not allow the crystal to have a constant temperature for every orientation. A study of the temperature variation was done, and reflections with an orientation corresponding to a temperature deviation greater than 0.5 °C from the mean were rejected (588 for the small crystal and 1633 for the large crystal).

Neutron Data Collection. Measurements were carried out on the four-circle diffractometer D8 situated at the high flux beam reactor of the Institut Laue-Langevin. The cryostat used was a closed loop displex refrigerator and did not allow the mounting of a crystal prepared elsewhere. So crystals were grown in situ using a vacuum shield where the crystal was directly visible (Figure 1). The aluminum pin which fixes the crystal in the quartz tube was used as thermal contact. The cell parameters determined by least-squares refinement based on 12 reflections ($18° < \theta < 38°$) agree with the values determined by X-rays within two standard deviations.

The experimental conditions for the data collection are summarized in Table I, and information pertinent to the remainder of the data treatment is given in Table II.

Data Processing. The data were reduced to structure factors in two different ways following the data collection techniques.

In the X-ray case a scan was used where direct integration was done during the measurement, and the background was estimated from stationary counts on each side of the peak.[9] For the neutron case the background was determined from the step-scan recorded profiles in such a way that the relative error in the intensity is minimized, followed by a correction of the peak width to reduce the known bias of this method.[10]

Absorption corrections were made using numerical integration over the volume of the crystal.[11] The cylindrical crystals were approximated by columns with eight faces. The absorption coefficients in the neutron case were assumed to come entirely from incoherent scattering of the hydrogen atoms. The variation of the transmission factors is given in Table II. The symmetry-related reflections were averaged and the corresponding estimated standard deviation was changed accordingly. At this stage an examination of the discrepancies between the equivalent reflections was computed, and the results are reported in Table II.

Structure Refinements. Neutron scattering lengths and X-ray form factors were taken from the International Tables.[12] The refinements were performed on F^2 with a weighting scheme described in Table II. The X-ray data obtained for the two crystals were used in separate refinements and then together. Secondary extinction effects were found to be negligible for the X-ray data, but an isotropic extinction parameter was included in the refinement using the neutron data.

Results

Atomic and thermal motion parameters obtained from the different structure refinements are compared in Table III. As expected the X-ray parameters of the hydrogen atom are not well determined, especially not from the high-order data recorded on the large crystal. Neutron and high-order X-ray parameters of the oxygen atom are in good agreement. Distances and angles are reported in Table IV together with those obtained by Busing and Levy[5] at −20 °C. We see once more the well-known effect of X-ray diffraction in the localization of the hydrogen atom: a shortening of the oxygen–hydrogen bond length. The H_2O_2 is not affected by the difference in temperature except by a very small change in the O–O–H angle. The main change appears in the distance between the two oxygen atoms in the hydrogen bond. This is normally followed by a lengthening of the oxygen–hydrogen bond, but in the present case the effect is of the same order of magnitude as the apparent contraction of the bond coming from the use of a centrosymmetric model for the thermal motion.[13]

The Deformation Electron Density. The electron density was analyzed using deformation density maps defined as

$$\Delta\rho = \rho_{obsd} - \rho_{calcd}$$

0002-7863/80/1502-1298$01.00/0

Table I. Experimental Data[a]

	X-ray	neutron
temp, K	110	
wavelength, Å	0.711	0.727
cell dimension a, Å	4.0162 (2)	4.004 (8)
c, Å	7.8545 (12)	7.832 (13)
scan mode	$\omega/2\theta$ (direct integration)	$\omega/2\theta$ (37 points step scan)
scan width, deg		
angle θ	0 17 35 53 70	0 10 20 30 45
low-angle side	0.50 0.75 1.10 1.50 2.00	2.1 2.3 2.7 3.2 3.7 (total)
high-angle side	1.50 1.50 1.50 1.55 1.80	
2θ range, deg	0-100 (SC) and 90-136 (LC)	0-82
standard reflections	2,0,5 0,2,5 3,0,1	5,0,1 2,0,6 −3,1,3
interval between standards	50	25
detector aperture, mm	5	14
crystal to detector distance, mm	230	340

[a] SC indicates the small crystal; LC indicates the large crystal. Standard deviations are here and throughout the paper indicated in parentheses in units of the last digit.

Table II. Summary of Data Treatment[a]

	X-ray	neutron
no. of reflections	4800 (SC) 3850 (LC)	910
max and min absorption correction	0.95-0.96 (SC) 0.90-0.93 (LC)	0.66-0.68
max no. of symmetry-equiv reflections measured	8	4
no. of symmetry-independent reflections measured	439 (SC) 333 (LC)	264
agreement factor $R = \Sigma\lvert F_o^2 - \bar{F}_o^2\rvert/\Sigma F_o^2$	0.03 (SC) 0.09 (LC)	0.12
weighting scheme $\sigma = (\sigma_o^2 + k(F_o^2)^2)^{1/2}$, k	0.0005 (SC) 0.0009 (LC)	0.0022
reflections rejected for	$F^2 < 0$	$F^2 < 0$
no. of reflections in refinement (NR)	420 (SC) 317 (LC)	240
no. of parameters refined (NV)	19 (SC) 14 (LC)	20
smallest extinction factor		0.76
agreement factors		
$R_F = \Sigma\lvert F_o - F_c\rvert/\Sigma F_o$	0.039 (SC) 0.039 (A) 0.036 (LC)	0.063
$R_{wF}^2 = [\Sigma w(F_o^2 - F_c^2)^2/\Sigma(wF_o^2)^2]^{1/2}$	0.057 (SC) 0.060 (A) 0.038 (LC)	0.077
$S = [\Sigma w(F_o^2 - F_c^2)^2/(\mathrm{NR} - \mathrm{NV})]^{1/2}$	1.64 (SC) 1.59 (A) 0.92 (LC)	0.91

[a] SC indicates small crystal; LC indicates large crystal; A indicates all data. F_o and F_c are observed and calculated structure amplitudes. σ_o is standard deviation of F_o^2, $w = 1/\sigma^2$; $\bar{F}_o$ is the mean of the symmetry-related F_o.

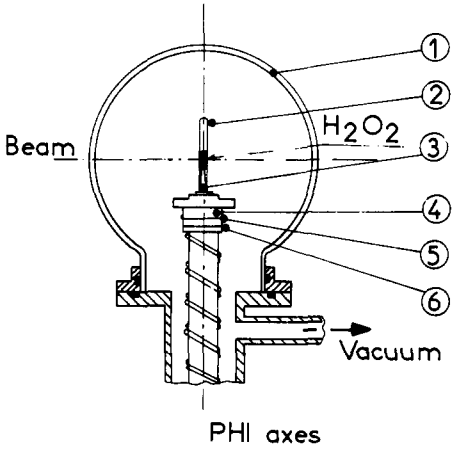

Figure 1. Cryostat used for neutron diffraction experiment. The cold tip is a closed-loop one-stage refrigerator[24] (Air Products, Model C-1003): 1, quartz cover; 2, quartz tube; 3, aluminum pin; 4, cold tip; 5, thermocouple; 6, heater.

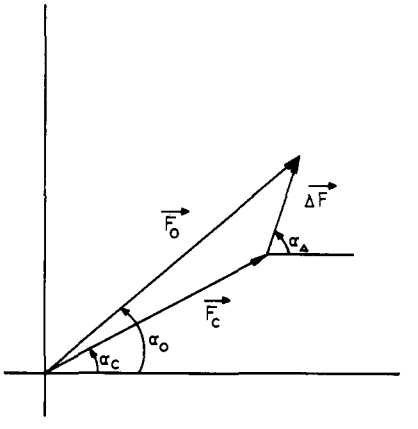

Figure 2. Diagram showing the relationships between the structure factors in the noncentrosymmetry case. The calculated structure factor F_c is based on spherical atoms. The amplitude of F_o is known from measurements and the phase α_o is obtained from a structure refinement.

using observed structure amplitudes for calculation of ρ_{obsd} and employing atomic positions and thermal parameters either from refinements of the X-ray data or from the neutron analysis together with spherical atomic scattering factors to obtain ρ_{calcd}. The two types of deformation are termed $\Delta\rho$(X-X) and $\Delta\rho$(X-N), respectively. As the structure is noncentrosymmetric the phasing of the observed structure amplitudes can create difficulties. We choose phases from a conventional refinement of the X-ray data used in the calculation of ρ_{obsd}. Although this type of refinement can lead to unrealistic atomic parameters, it is assumed to describe the density well, and thus supply acceptable phases for the structure factors. In practice we would calculate the deformation density as

$$\Delta\rho(x, y, z) = \sum\Delta F \cos(2\pi(hx + ky + lz) - \alpha_\Delta)$$

where the summation is over all structure factors ΔF with indices hkl. Figure 2 defines in a vector diagram the different quantities, where the phase α_o of the structure factor F_o is obtained as described above. For a structure factor fixed by symmetry F_o and F_c are collinear and $\alpha_o = \alpha_c$ if ΔF is small compared to F_c. We could assume that all phases are deter-

Table III. Final Atomic Parameters[a]

		X-ray			neutron	
		small crystal	large crystal	total		Busing and Levy[5] (253 K)
	x	0.07692(12)	0.07609(5)	0.07635(7)	0.0762(3)	0.0731(4)
	y	0.16767(12)	0.16746(5)	0.16756(7)	0.1670(3)	0.1670(4)
	z	0.22064(5)	0.22041(3)	0.22053(4)	0.2204(1)	0.2213(2)
oxygen	U_{11}	0.01065(16)	0.00997(7)	0.01038(8)	0.0096(4)	0.0209(7)
	U_{22}	0.01123(17)	0.01061(8)	0.01100(8)	0.0107(4)	0.0217(8)
	U_{33}	0.01115(11)	0.01030(5)	0.01085(8)	0.0120(3)	0.0194(7)
	U_{12}	−0.00122(13)	0.00010(3)	−0.00011(5)	−0.0001(4)	0.0021(6)
	U_{13}	−0.00042(15)	−0.00044(4)	−0.00048(6)	0.0004(3)	−0.0013(6)
	U_{23}	0.00145(15)	0.00028(4)	0.00050(6)	0.0003(3)	−0.0005(6)
	x	−0.029(3)	−0.01(1)	−0.027(3)	−0.0483(7)	−0.0473(11)
	y	0.253(3)	0.30(1)	0.253(3)	0.2834(6)	0.2838(9)
	z	0.148(2)	0.14(1)	0.149(2)	0.1296(3)	0.1317(4)
hydrogen	U_{11}	0.029(9)	0.014(6)	0.028(8)	0.0245(9)	0.0410(17)
	U_{22}	0.015(8)	0.014(6)	0.014(7)	0.0203(9)	0.0362(19)
	U_{33}	0.028(6)	0.014(6)	0.032(6)	0.0245(7)	0.0288(9)
	U_{12}	0.018(6)		−0.018(6)	0.0018(7)	0.0034(16)
	U_{13}	0.003(7)		0.007(6)	−0.0038(7)	−0.0026(13)
	U_{23}	0.002(6)		0.002(6)	0.0072(6)	0.0077(14)

[a] The temperature factors are defined as $T_i = \exp(-2\pi^2(U_{11}a^{*2}h^2 + U_{22}b^{*2}k^2 + U_{33}c^{*2}l^{*2} + 2U_{12}a^*b^*hk + 2U_{13}a^*c^*hl + 2U_{23}b^*c^*kl)$. The present X-ray and neutron data are for a temperature of 110 K; the data of Busing and Levy are for 253 K.

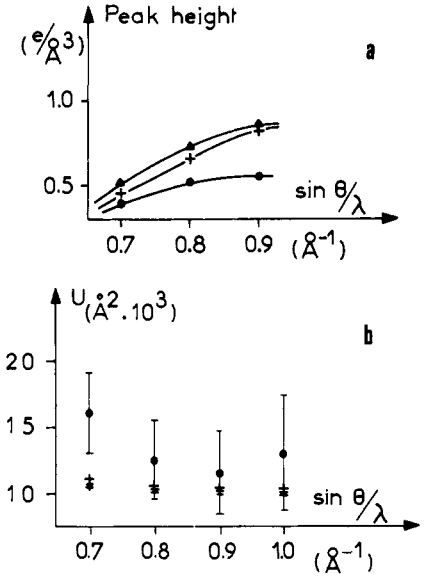

Figure 3. (a) Peak heights in the deformation map $\Delta\rho$(X-X) as a function of data cutoff expressed in $\sin\theta/\lambda$(Å^{-1}): ●, hydrogen-oxygen bond; ▲, lone pair involved in hydrogen bonding (lp_1); +, other lone pair (lp_2). (b) Thermal parameters from high-order refinements. The lower limit of data is indicated as $\sin\theta/\lambda$. · +, U_{ii} (i = 1, 2, 3) for oxygen; ●, isotropic U for hydrogen. The error bars corresponds to ±1 standard deviation.

mined this way, and calculate the density

$$\Delta\rho'(x, y, z) = \sum\Delta F' \cos(2\pi(hx + ky + lz) - \alpha_c)$$

where $\Delta F'$ is the difference between the amplitudes of F_o and F_c. If F_o and F_c are much larger than ΔF, then we can approximate $\Delta F' = \Delta F \cos(\alpha_\Delta - \alpha_c)$ and setting $\phi = \alpha_\Delta - \alpha_c$ we get

$$\Delta\rho'(x, y, z) = \sum\Delta F \cos\phi \cos(2\pi(hx + ky + lz) - \alpha_\Delta + \phi)$$

For ΔF being small all values of ϕ are equally likely, and we can then estimate the expected value of $\Delta\rho'$ as

$$\langle\Delta\rho'(x, y, z)\rangle = \frac{1}{2\pi}\int_{-\pi}^{\pi}\Delta\rho'\,d\phi = \frac{1}{2}\Delta\rho(x, y, z)$$

Test calculations were carried out for data with $\sin\theta/\lambda < 0.7$ Å^{-1}. Because of the high symmetry as much as 60% of the phases had $\alpha_o = \alpha_c$, so 60% of the contributions would be the same in $\Delta\rho'$ and $\Delta\rho$. Therefore $\langle\Delta\rho'\rangle = 0.60\Delta\rho + \frac{1}{2} \times 0.40\Delta\rho = 0.8\Delta\rho$. For the maxima of the lone pairs discussed below we found a ratio $\Delta\rho'/\Delta\rho = 0.76$, indicating that $\Delta\rho$ has increased satisfactorily by the improved phasing. A shift of 0.1 Å in the peak position was observed between the two maps. Similar calculations for data with $\sin\theta/\lambda < 0.9$ Å^{-1}, where 54% of the phases are fixed, gave a value for $\Delta\rho'/\Delta\rho$ of 0.70 compared to the expected 0.77, so again the improvement was satisfactory. We can therefore believe that errors induced by the phasing are of the order of less than 10% of the deformation density. To bring ρ_{obsd} to an absolute scale a refinement of the scale factor was done using the atomic parameters for the determination of ρ_{calcd}.

As we include more and more terms in the calculation of $\Delta\rho$ the features in the maps get sharper and will eventually reach the values for infinite resolution.[14] Likewise the noise level will increase. We looked at the peaks in the maps for a series of cutoff values (expressed in $\sin\theta/\lambda$), and the result is shown in Figure 3a. At $\sin\theta/\lambda$ = 0.9 Å^{-1} we seem to approach the values for infinite resolution, and we chose this value for further analysis.

When the calculated maps were based on X-ray parameters, these were obtained from high-order data going beyond the

Table IV. Distances (A-B), Angles (∠A-B-C), and Dihedral Angles (A-B-C-D)

		neutron	
	X-ray 110 K	110 K	(Busing and Levy,[5] 253 K)
O-O	1.461(3)	1.458(4)	1.453(7)
O-H	0.77(9)	0.988(3)	0.988(5)
H···O	1.98(10)	1.786(5)	1.825(6)
O····O	2.758(6)	2.761(5)	2.799(8)
∠O-O-H	99.5(18)	101.9(1)	102.7(3)
∠O-O···O	94.4(5)	94.5(3)	94.8(2)
∠O-H···O	172.3(25)	168.4(2)	167.6(4)
H-O-O-H	93.3(22)	90.2(4)	90.2(6)
O···O-O···O	127.2(4)	126.6(5)	127.4(4)
H-O-O···H	124.3(25)	120.5(5)	120.8(4)

[a] Distances are in ångstroms, angles in degrees. Dotted lines indicate hydrogen bond.

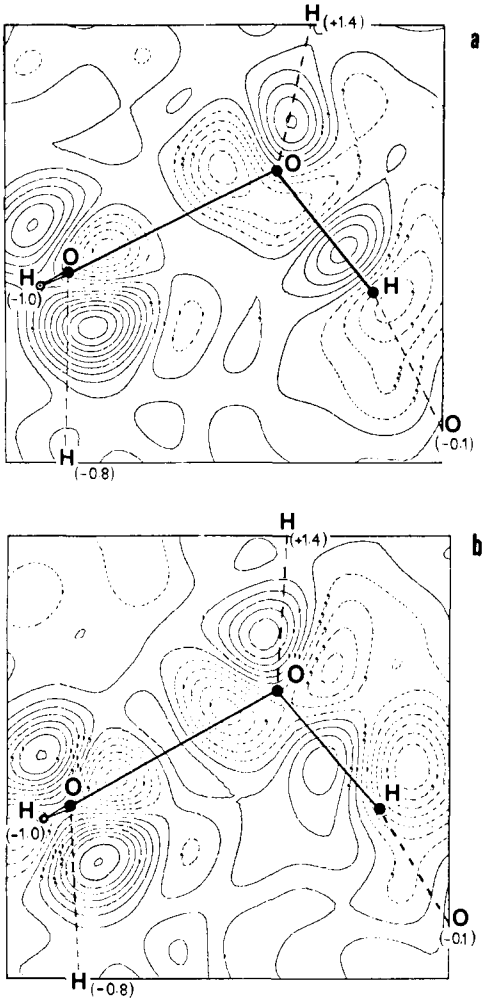

Figure 4. (a) $\Delta\rho$(X-N). (b) $\Delta\rho$(X-X). Broken contours corresponds to negative electron density. Lowest unbroken contour corresponds to zero density. Interval between contours 0.1 e/Å^3.

above-mentioned cutoff. Figure 3b shows the results using various lower limits. For the highest lower limit the (isotropic) thermal parameter of hydrogen is not well defined because of the small core contribution of hydrogen at high scattering angles. No error maps were calculated. The error in a general point, at a distance of more than approximately 0.3 Å, can, however, be assumed to come mainly from errors in the observed structure amplitude,[15] and the value for this error was found to be 0.06 e/Å^3.

Discussion

The O–O–H Plane. The deformation density maps for the O–O–H plane are represented in Figures 4a ($\Delta\rho$(X-N)) and 4b ($\Delta\rho$(X-X)). As discussed above it was difficult to determine the thermal motion of the hydrogen atom from the X-ray data, so there are large differences between the two maps in the region of the hydrogen–oxygen bond. The common feature is, however, the absence of positive electron density between the oxygen atoms. This is in contrast to what is generally observed, but it seems as well in disagreement with the requirement of balance of the electrostatic forces on the nuclei, which can be estimated using the Hellmann–Feynman electrostatic theorem.[16,17] We have described the density as $\rho = \rho_P + \Delta\rho$, where ρ_P is the sum of spherical electron densities, and the force on the nuclei is a sum of the two forces, F_p and F_Δ, corresponding to these densities, respectively.[17] F_p is always repulsive when one atom penetrates into the charge cloud of another atom, so in order to have cancellation of forces on the oxygen, and thus

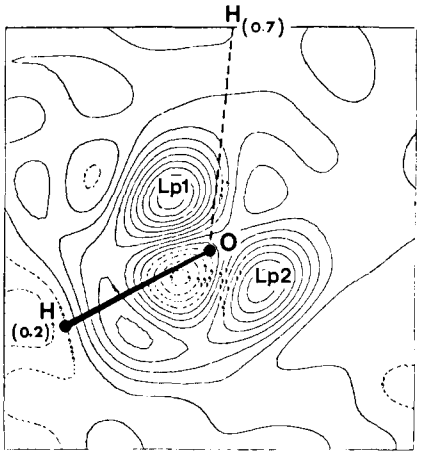

Figure 5. Section of $\Delta\rho$(X-N) orthogonal to the oxygen–oxygen bond through the oxygen atom. Contours as in Figure 4.

a stable molecule, F_Δ must be attractive. This is most easily obtained by placing electrons between the nuclei, and this corresponds to what is generally observed, especially in various types of carbon–carbon bonds which constitute the major part of the presently observed deformation densities.

If the atoms involved in bonding have electron-rich valence shells, two things might happen, which reduce the amount of density between the nuclei. First, the interatomic distance can be so large that the penetration of one nucleus into the charge cloud of the other atom is limited, and this reduces F_p. For oxygen the van der Waals radius is around 1.40 Å, so this effect is going to be small. Secondly, as the atoms approach each other transport of electrons to the internuclear region would violate the Pauli exclusion principle, and electrostatic balance is then obtained by polarization of the core and the π-bonding orbitals[17] toward this region. We are not able to observe the polarization near the core, as the errors are too large,[18] but we do find the π-type density (involved in formation of the lone pairs) shifted toward the bonding region. A recent calculation of the difference density[7] shows the same general features, and these are found as well in bonds involving atoms with electron-rich valence shells such as nitrogen–oxygen bonds in *p*-nitropyridine *N*-oxide,[19a] uronium nitrate,[19b] *n*-phenyl sydnone,[19c] and in the carbon–chlorine bond in 2-amino-5-chloropyridine.[19d] So if we use deformation density maps to get a qualitative idea of the electronic rearrangement during bonding this seems to manifest itself either as a charge cloud in the bond center or as polarized lone pairs depending roughly on the number of valence electrons involved in bonding.

The Oxygen Lone Pairs and the Hydrogen Bond. Figure 5 shows a section of $\Delta\rho$(X-N) through the oxygen lone pair region orthogonal to the oxygen–oxygen axis. Three maxima are found in this region. One of these corresponds to the intramolecular oxygen–hydrogen bond; the other two are taken to indicate the location of the lone-pair distributions, lp_1 and lp_2. Table V summarizes the positions of the lone-pair maxima as well as distances and angles around the oxygen atom.

For the following discussion an estimate of the accuracy of the quoted angles is of importance. If we take a parallel to normal structure analysis, we know that the atomic positions are generally quite insensitive to the quality of the data, but that thermal parameters act as "error sponges". We can therefore expect maxima of well-shaped peaks in $\Delta\rho$ to be quite independent of the actual set of data used, and attempts to shift atoms in a $\Delta\rho$ calculation[19a] gave no indication of sensitivity to the chosen atomic positions within reasonable limits. Likewise a comparison of the lone-pair angle C–O–lp in four carboxyl groups[19a] showed these to lie in the range of 111–121°, indicating the error to be approximately 5°.

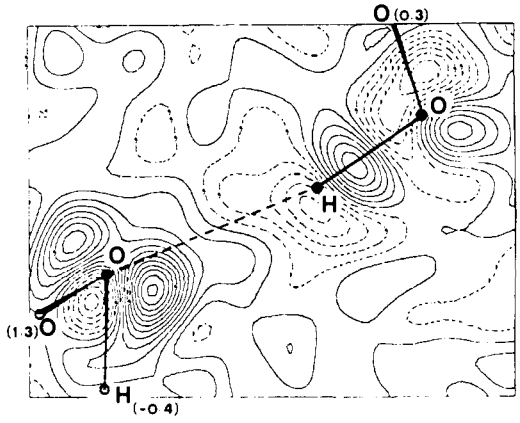

Figure 6. Section of $\Delta\rho$(X-N) through the atoms O···H-O involved in the hydrogen bond. Contours as in Figure 4.

Table V. Configuration of the Lone Pairs[a]

		x	y	z	max, e/Å^3
lp_1		0.043	0.233	0.246	0.99
lp_2		0.147	0.116	0.204	0.88
O-lp_1	0.36				
O-lp_2	0.37				
lp_1···H	1.53				
lp_1···O	2.52				

∠O-O-lp_1	102.0	∠lp_1-O-lp_2	150.7
∠O-O-lp_2	94.0	∠lp_1···H-O	176.7
∠H-O-lp_1	82.9	H-O-O-lp_1	6.7
∠H-O-lp_2	113.7	H -O-O-lp_2	209.0

[a] The positions (x, y, z) are given in fractions of the unit cell axis. Nomenclature as in Table IV.

In the gaseous state the dihedral angle ϕ(H-O-O-H) is 111.5°.[21] The oxygen is expected to have an sp^3 hybridization, so the hydrogen atom and a lone pair are nearly eclipsed[22] and calculations show[6,22] that minima in the potential energy as a function of ϕ are only obtained when lone-pair electron densities are described accurately.

We observe in the solid state a distorted sp^3 configuration with angles O-O-H, O-O-lp_1, and H-O-lp_2 in a reasonable agreement with the tetrahedral angles, but with lp_1 well offset from the ideal position. However, we still have eclipse of the hydrogen atom with lp_1 with a dihedral angle lp_1-O-O-H of only 6.7°. The change in ϕ comes from the involvement of the hydrogen in a hydrogen bond, where the electron donor is the oxygen atom. Figure 6 shows a section of $\Delta\rho$(X-N) through the atoms O···H-O. The features are typical for a long hydrogen bond, where the main interaction is of electrostatic nature,[23] and as often observed the oxygen-hydrogen bond points toward a region of high electron density, which we term the lone pair, and which in this case is lp_1. Normally discussion of this type of directionality can only indicate trends, as many interactions and constraints are operating when molecules pack, and it is unlikely that the oxygen-hydrogen bond can orient itself freely. In a molecule as simple as H_2O_2 it might, however, still be worthwhile, and in Figure 7 we have shown in a projection the positions involved in bonding.

In a hydrogen bond system O-lp···H-O we can at the extreme either have the oxygen-lone pair pointing toward the hydrogen atom ("lone-pair directionality"), and the hydrogen bond interactions will then dominate over intraatomic interactions, or we can have the oxygen-hydrogen bond pointing toward the lone pair, and we have "hydrogen directionality" and dominating intermolecular interactions. In H_2O_2 the first case would correspond to lp_1 moving onto the line O···H and not only creating a nearly perfect tetrahedron, but reducing

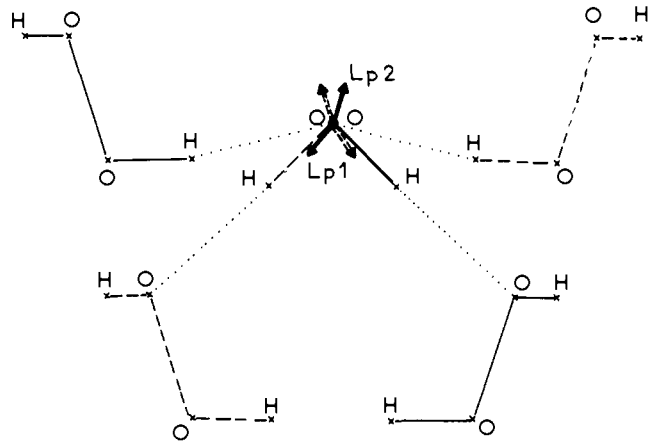

Figure 7. Projection of atom and lone-pair positions onto a plane orthogonal to the oxygen-oxygen axis. Continuous lines corresponds to one end of molecule, broken lines to other end, and dotted lines to hydrogen bond.

as well the lone pair-hydrogen distance. As this is contrary to our observations of a small dihedral angle lp_1-O-O-H and an angle O-H···lp_1 of 176.6°, we conclude that H_2O_2 satisfies both the concept of intramolecular domination of the lone pair and "hydrogen directionality" as defined above. In the simple picture of hydrogen bonding we see electrons transferred from the electron donor, oxygen, to the proton donor, hydrogen, so in the present case we would expect lp_1 to be smaller than lp_2, in contrary to observations. We do, however, not know whether lp_1, eclipsed to hydrogen in the gas state, is much larger than lp_2, but it seems reasonable to conclude even then that the effect on lp_1 from hydrogen bonding is small. In addition we can note that the hydrogen-bond interactions are obviously anharmonic as the O···H distance contracts as much as 0.028 Å when the crystal is cooled 140 °C.

Conclusion

The present study has revealed an absence of positive charge density in the region between the oxygen atoms of a deformation density map $\Delta\rho$. We do not believe this to be an artifact of experimental error, as large and well-defined densities are found between oxygen and hydrogen as well as in the lone-pair regions of oxygen, but rather a consequence of our technique for calculations of $\Delta\rho$. For valence-electron-rich atoms the sum of densities of the spherical atoms could well be nearly as large as the density of electrons in the binding molecular orbitals, and we would then using difference techniques mainly observe rearrangements in the π-bonding regions and only very small charge clouds at the bond center. It does, however, indicate that the flow of electrons into the binding region is smallest for the heavier first-row atoms as found by Bader et al.[16] Indeed, for all observed bonds between atoms involving more than ten electrons in the valence shell we do find an absence of electron in the bonding region of $\Delta\rho$ corresponding to the case where all bonding molecular orbitals are filled, and where electrons are as well found in the antibonding orbitals. If we use prepared "valence atoms" [16] in preparation of $\Delta\rho$ the picture is more consistent through the first-row atoms, showing in all cases an accumulation of electrons at the bond midpoint. This is, however, not a practical approach when we want to study arrangements in complicated molecules.

One hydrogen bond is present in the structure, and the molecular configuration indicates that this influences the dihedral angle ϕ, while at the same time the energy-favorable interaction between the hydrogen and a lone pair is maintained.

Acknowledgments. We thank Professor P. Coppens for discussion, which led us to undertake this study. We are in-

debted to Mr. P. Simms for the design of the neutron cryostat.

Supplementary Material Available: A listing of structure factors (7 pages). Ordering information is given on any current masthead page.

References and Notes

(1) On leave from Laboratoire de Chimie de Coordination du CNRS, 31030 Toulouse Cedex, France.
(2) (a) L. J. Thenard, *Ann. Chim. Phys.*, **8**, 306 (1818); (b) P. A. Giguere, "Compléments au Nouveau Traité de Chimie Minérale," A. Pacault and G. Pannetier, Eds., Masson et Cie, Paris, 1975.
(3) W. G. Penney and G. B. B. M. Sutherland, *Trans. Faraday Soc.*, **30**, 898 (1934); *J. Chem. Phys.*, **2**, 492 (1934).
(4) S. C. Abrahams, R. L. Collin, and W. N. Lipscomb, *Acta Crystallogr.*, **4**, 15 (1951).
(5) W. R. Busing and H. A. Levy, *J. Chem. Phys.*, **42**, 3054 (1965).
(6) T. H. Dunning Jr. and N. W. Winter, *J. Chem. Phys.*, **63**, 1847 (1975).
(7) P. Coppens and E. D. Stevens, *Adv. Quantum Chem.*, **10**, 1 (1977).
(8) P. A. Giguere, I. D. Liu, J. S. Dugdale, and J. A. Morrison, *Can. J. Chem.*, **32**, 117 (1954).
(9) W. Hoppe, *Angew. Chem.*, 77, 484 (1965).
(10) M. S. Lehmann and F. K. Larsen, *Acta Crystallogr., Sect. A*, **30**, 580 (1974).
(11) P. Coppens, L. Leiserowitz, and D. Rabinovich, *Acta Crystallogr.*, **18**, 1035 (1965).
(12) "International Tables for X-ray Crystallography", Vol. IV, Kynoch Press, Birminham, England, 1974.
(13) W. R. Busing and H. A. Levy, *Acta Crystallogr.*, **17**, 142 (1964).
(14) M. S. Lehmann and P. Coppens, *Acta Chem. Scand., Ser. A*, **31**, 530 (1977).
(15) E. D. Stevens and P. Coppens, *Acta Crystallogr., Sect. A*, **32**, 915 (1976).
(16) R. F. W. Bader, W. H. Henneker, and P. E. Cade, *J. Chem. Phys.*, **46**, 3341 (1967).
(17) F. L. Hirshfeld and S. Rzotkeiwicz, *Mol. Phys.*, **27**, 1319 (1974).
(18) B. Rees, *Acta Crystallogr., Sect. A*, **32**, 483 (1976).
(19) (a) P. Coppens and M. S. Lehmann, *Acta Crystallogr., Sect. B*, **32**, 1777 (1976); (b) G. de With, S. Harkema, and D. Feil, *Acta Crystallogr., Sect. A*, **31**, S227 (1975); (c) H. Hope, Collected Abstracts, XI International Congress of Crystallography, 1978, p S20; (d) Å. Kvick, R. Thomas, and T. F. Koetzle, *Acta Crystallogr., Sect. B*, **32**, 224 (1976).
(20) N. K. Hansen and P. Coppens, *Acta Crystallogr., Sect. A*, **32**, 909 (1978).
(21) R. L. Redington, N. B. Olson, and P. C. Cross, *J. Chem. Phys.*, **36**, 1311 (1962).
(22) P. B. Ryan and H. D. Todd, *J. Chem. Phys.*, **67**, 4787 (1977).
(23) I. Olovsson, "Proceedings of NATO Summer School, Arles, 1978," Plenum Press, New York, in press.
(24) P. Simms, M. S. Lehmann, and S. Mason, submitted for publication.

Spectroscopic and Structural Investigation on the Pentachloro- and (Mixed-pentahalo)cuprates(II) of the *N*-(2-Ammoniumethyl)piperazinium Cation. The First Case of Monomeric Pentahalocuprate(II) Having Square-Pyramidal Structure. Crystal and Molecular Structure of the (*N*-(2-Ammoniumethyl)piperazinium) Pentachlorocuprate(II) Dihydrate

L. Antolini,[1a] G. Marcotrigiano,[1b] L. Menabue,[1a] and G. C. Pellacani*[1a]

Contribution from the Consiglio Nazionale delle Ricerche, Rome, Italy, Istituto di Chimica Generale e Inorganica, University of Modena, 41100 Modena, Italy, and Istituto di Chimica, Facolta di Medicina-Veterinaria, University of Bari, 70126 Bari, Italy.
Received August 8, 1979

Abstract: Some compounds of the type $(N(2amet)pipzH_3)CuCl_mBr_{5-m}\cdot nH_2O$ ($N(2amet)pipzH_3$ = *N*-(2-ammoniumethyl)-piperazinium cation; $m = 5$ and $n = 2$; $m = 4, 3, 2, 1$ and $n = 1$) were prepared and investigated by means of X-ray powder, electronic and vibrational spectra, and magnetic moments. For one of them, $(N(2\text{-amet})pipzH_3)CuCl_5\cdot 2H_2O$, the crystal structure was also determined by three-dimensional X-ray diffraction. The substance crystallizes in space group $P2_1/a$ with lattice constants $a = 17.991$ (6) Å, $b = 9.249$ (3) Å, $c = 9.560$ (4) Å, $\beta = 98.14$ (5)°, and $Z = 4$. The intensity data were collected with a Philips PW 1100 automatic four-circle diffractometer using Mo Kα radiation. The structure was solved by three-dimensional Patterson and Fourier methods and parameters were refined by least-squares calculations to a conventional *R* factor of 3.4% for 1652 independent reflections [$I > 3\sigma(I)$]. The structure consists of discrete $CuCl_5^{3-}$ and $[N(amet)pipzH_3]^{3+}$ ions and of two water molecules of crystallization. The $CuCl_5^{3-}$ anion has a slightly distorted square-pyramidal coordination. A very complex network of hydrogen bonds was observed and considered to be responsible for this new geometry for CuL_5 (L = unidentate ligand) complexes. The magnetic and spectroscopic results for all the compounds indicate that they are isomorphous. The far-IR and Raman spectra of the square-pyramidal $CuCl_5^{3-}$ ion were also discussed and assigned. The presence of strong hydrogen bonds was also observed in the infrared spectra.

Introduction

The copper(II) halides are rather interesting, showing a great variety of coordination numbers and geometries,[2] and, as they contain unidentate ligands, are also probably of the greatest potential interest from an electronic structural viewpoint.

In the case of pentacoordinated complexes, although differences in energy between trigonal bipyramidal and square-pyramidal structures should be small, as a general tendency, we can expect the trigonal bipyramidal structure to be favored with respect to the square-pyramidal one, whenever the five ligands are equivalent or nearly so with no particular steric constraints.[3,4] In accordance with these considerations, the only known monomeric pentahalocuprate ions (CuX_5^{3-} (X = Cl, Br) and $CuCl_2Br_3^{3-}$) present trigonal bipyramidal structures,[5,6] and other pentacoordinated chlorocuprates(II), such as $(CH_3)NH_2CuCl_3$,[7] $PhCH_2CH_2NMeH_2CuCl_3$,[8]

0002-7863/80/1502-1303$01.00/0